Geophysical Prospecting, 2002, **50**, 475–485

Seismic endoscopy: multi-offset multi-azimuth imaging around boreholes – data processing and experimental results

Florence Nicollin,* Frédéric Conil and Dominique Gibert

Géosciences Rennes, UMR 6118 CNRS, Université de Rennes 1, 35042 Rennes Cedex, France

Received April 2001, revision accepted March 2002

ABSTRACT

An acoustic method, called seismic endoscopy, able to perform 3D imaging around shallow-depth boreholes is presented. A probe, composed of an isotropic source and a directional receiver working in the 20–100 kHz frequency range, provides images of cylindrical volumes having radii of a few metres, with an accuracy of centimetres and 25° azimuthal directivity. In order to obtain clear images of the medium discontinuities, multi-offset and multi-azimuth data acquisition allows specific algorithms to be used to determine vertical directivity correction, azimuthal focusing and reflected wave enhancement by cancellation of the tube waves. The method is tested with data acquired in an acoustic tank and with synthetic data. Initial experimental results at a test site demonstrate the performance of the seismic endoscopy probe.

INTRODUCTION

Seismic endoscopy is an acoustic method for performing imaging at distances of a few metres around shallow-depth boreholes with an accuracy of centimetres. A first probe was designed, constructed and tested in an acoustic tank, with basic imaging algorithms (Valéro, Sarraco and Gibert 2001). As shown in Section 1, the particular acquisition geometry of this kind of apparatus yields data depending on three spatial parameters: the location of the probe in the borehole, the source–receiver distance (commonly called the offset), and the earring azimuth. In previous work, the processing algorithms did not take the offset parameter into account, focusing on the non-conventional azimuth parameter. Here, we present imaging processing based on the entire time–space dependence of the data. After presenting the directivity obtained with a new receiver module, Section 2 demonstrates the processing performed in order to obtain an image that is as accurate as possible. Azimuthal refocusing based on the horizontal directivity and correction of vertical directivity are illustrated on data recorded in an acoustic tank for directivity measurements. The processing carried out to achieve reflected wave enhancement is then shown using synthetic data. In Section 3, we present experimental results obtained at a test site, where limited reflectors surround the probe at various distances and azimuths, using water as the propagation medium. The test site provides a controlled model at typical scales of interest, i.e. a cylinder several metres high with a radius of metres, around a borehole, 12 cm in diameter.

*E-mail: florence.nicollin@univ-rennes1.fr

1 ACQUISITION GEOMETRY

1.1 Principle of the method

The probe is composed of a multidirectional controlled source and a directional receiver working in the 20–100 kHz frequency range (Fig. 1). Both source and receiver are acoustic transducers sensitive to pressure variations in water, thus requiring a fluid-filled borehole. The directivity in reception is obtained by embedding a standard isotropic piezo-electric transducer (Brüel & Kjær 8103) in a cylinder of absorbent material with a narrow window. In previous work (Valéro *et al.* 2001), two transducers were embedded in the same cylinder, causing mutually diffracted signal at each of the receivers. By moving the receiver along the axis of the probe, the source–receiver distance ξ, called offset as in

conventional surface seismic, may be set between 20 and 80 cm with an accuracy of better than 1 cm. By rotating the probe, the earring window of the receiver may be orientated at any azimuth θ between 0° and 360°. At each depth z, the source fires for all offsets and azimuths. Thus, the recorded data contain echoes reflected under various angles of incidence (common-azimuth θ_j, common-shot z_l gathers $s_{\theta_j z_l}(t, \xi)$) and coming from different directions (common-offset ξ_k, common-shot z_l gathers $s_{\xi_k z_l}(t, \theta)$). By changing the depth of the probe in the borehole, a multiple coverage survey is performed as in classical seismic, providing common-midpoint (CMP) z_m gathers $s_{\theta_j z_m}(t, \xi)$ at each earring azimuth. This particular acquisition geometry offers the possibility to process data in a 5-dimensional space (amplitude, time t, depth z, offset ξ, azimuth θ), with the aim of an ultimate 3D image of the acoustic discontinuities present in a cylindrical volume surrounding the borehole.

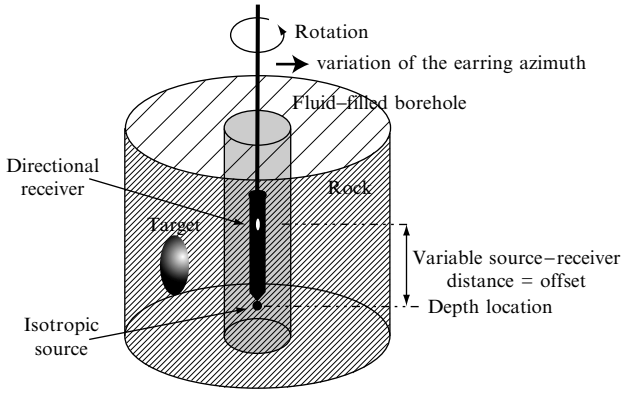

Figure 1 Principle of the 3D seismic endoscopy probe: a multidirectional source and an azimuthally directional receiver, working in the 20–100 kHz frequency range, image targets located around the borehole, using reflected echoes.

1.2 Expected content of the data

In addition to reflected echoes from the medium, the data contain both waves refracted at the borehole–formation interface, i.e. first arrivals, and large tube waves arriving later and blurring the reflected waves (Paillet and Cheng 1991). The tube waves propagate along the borehole boundary and in the water filling the borehole. For a perfectly cylindrical borehole and if the probe is precisely centred in the borehole, the refracted waves and the tube waves do not depend on the azimuth. Thus, in the (t, θ, ξ) space, the wavetrains describe conical surfaces: equal-time arrivals on common-offset gathers and arrivals along straight lines of slopes equal to the apparent slowness on common-azimuth gathers. In the case of a borehole with imperfect walls and/or if the probe is not precisely centred in the borehole, all wavetrains have a similar undulating shape on the common-offset gathers. Moreover in this case, the tube waves may have a varying amplitude over the whole azimuthal range due to destructive interference between the vibrating modes. In the (t, θ, ξ) space, the reflected wavetrains describe

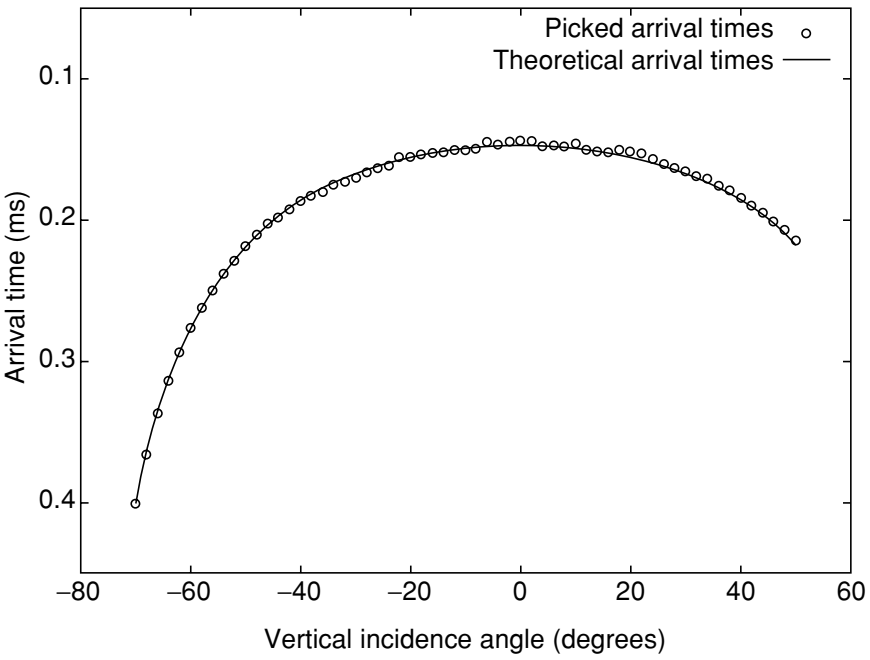

Figure 2 Arrival times picked on data recorded in an acoustic tank with a point source located at a variable depth from the receiver, and theoretical arrival times computed with a horizontal distance $d =$ 218 mm and a propagation velocity $V_w =$ 1480 m/s.

hyperbolic surfaces: classical reflection hyperbola in time–offset planes, limited to the azimuthal directivity angle and with identical arrival times whatever the azimuth in this angular area, as shown at the end of the next section.

1.3 Assessment of the probe directivity

We performed a simple experiment in a water tank in order to measure the directivity of the receiver, in both horizontal and vertical planes. A small piezo-electric source is located at a horizontal distance d of about 20 cm from the probe, at different depths, thus causing the angle of incidence to the probe receiver to vary between -70° and $+50^\circ$ in 10° steps. At each vertical location, the probe rotates from -90° to $+90^\circ$ in 2° steps. A complementary experiment is carried out every 2° vertical incidence at the zero azimuth (i.e. the receiver window in front of the source) in order to determine precisely the propagation velocity and the source–receiver distance. Another experiment, carried out with a larger horizontal distance, between -90° and $+90^\circ$ azimuth at normal incidence, leads to an estimation of the amplitude attenuation. The source signal is a Ricker wavelet with central frequencies of 30, 50, 70 and 100 kHz.

Figure 2 shows the arrival times picked on the data of the complementary experiment made with a 100 kHz Ricker wavelet. By performing velocity analysis (minimization of the mean squared error between observed times and theoretical times), we determined the propagation velocity in water $V_w = 1480 \pm 5$ m/s, and the horizontal distance between source and receiver $d = 218 \pm 1$ mm. By comparing the experiments carried out at two different horizontal distances, between -90° and $+90^\circ$ azimuth at normal incidence and with a 100 kHz Ricker wavelet, the differences in arrival times correspond to a difference of 198 mm in horizontal distance with $V_w = 1480$ m/s. As expected, the attenuation is due only to geometric spreading ($A_1/A_2 = d_2/d_1$).

Figure 3 shows the directivity diagrams obtained at the four frequencies of the Ricker wavelet (30, 50, 70 and 100 kHz). The amplitudes are corrected for geometric spreading and are normalized to 1. The sampling steps are 2° in the azimuthal angle and 10° in the vertical angle of incidence. Although the receiver window has a square aperture of 2 cm (i.e. 60°) horizontal and vertical, all diagrams show a sharper directivity in the vertical plane than in the horizontal one. The directivity is better at higher frequencies and the arrival times are azimuthally independent over the

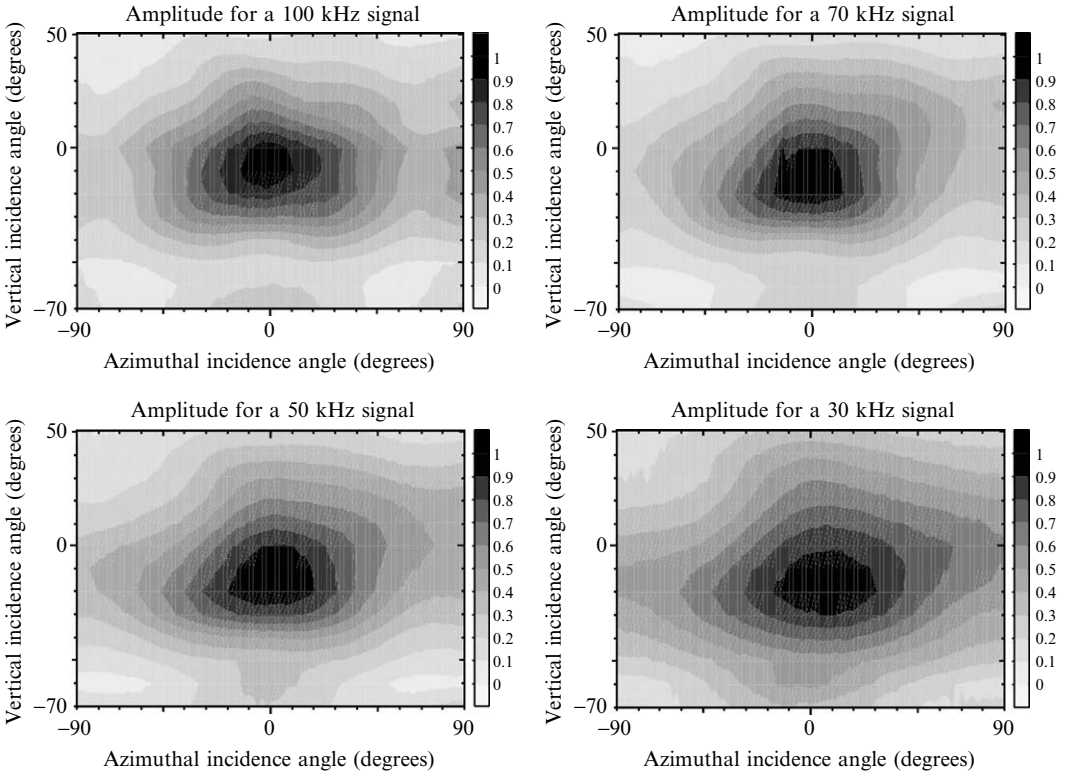

Figure 3 Directivity diagrams for several frequencies.

entire azimuthal range (see Fig. 5b for an example). This contrasts with a previous version of the probe which showed an azimuthal dependence of the arrival times (Valéro *et al.* 2001). These two observations suggest that the waves pass through the probe material surrounding the receiver without any significant delay but with a frequency-dependent absorption. The directivity curves will be used to perform amplitude correction with respect to the vertical angle of incidence and azimuthal focusing.

2 DATA PROCESSING

2.1 Amplitude corrections

The correction of geometric spreading may be done either with a classical gain factor (Clærbout 1985) or by weighting each trace by its corresponding distance travelled. The latter solution implies knowledge of the velocity law which can be obtained by carrying out velocity analysis on common-azimuth CMP gathers previously corrected with a rough gain factor.

The aim of the vertical directivity correction is to equalize the amplitude of the echoes recorded at various vertical angles of incidence. The correction is effective for angles of incidence of less than 50°, i.e. for reflectors located at a radial distance d larger than 8 cm for the 20 cm offset and larger than 34 cm for the 80 cm offset. The algorithm is based on amplitude curves measured in the vertical directivity experiment at positive vertical angles of incidence since, in the seismic endoscopy probe, the receiver is located above the source. A smooth curve from 0° to 50° in vertical angles of incidence (φ), obtained with moving average over 12° in φ, is extracted from the directivity diagram at azimuth 0°. The normalized inverse values provide a weighting curve $A^{-1}(\varphi)$, shown in Fig. 4(a) for the 100 kHz frequency. For angles of incidence larger than 50°, the curve $A^{-1}(\varphi)$ is equal to 1. The corrected traces are obtained by multiplying the recorded traces $s(t, \varphi_k)$ by the corresponding value $A^{-1}(\varphi_k)$. Data recorded at azimuth 0° during the directivity experiment at 100 kHz are shown in Fig. 4(b) after correction for geometric spreading, and the same traces, corrected for the vertical directivity, are shown in Fig. 4(c).

After data acquisition, the traces are grouped in CMP gathers $s_{\theta_j z_m}(t, \xi)$ and are NMO-corrected to give the shifted traces $s_{\theta_j z_m}(t', \xi)$, where t' corresponds to the two-way traveltime between the probe and a radial distance d for each sample: $2d_i = V_{ijm}.t'_i$ with V_{ijm} being the propagation velocity. Then, at each sample t'_i of a trace recorded with a given

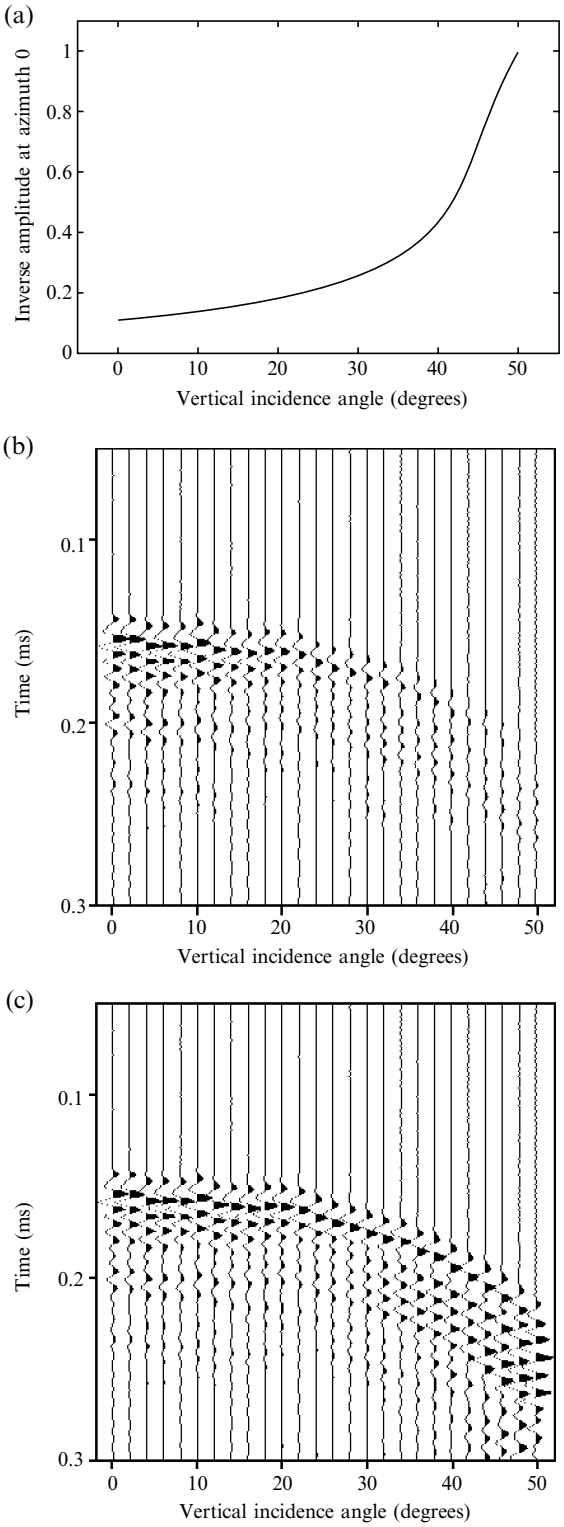

Figure 4 Correction of vertical directivity: (a) inverse of smoothed directivity curve at 100 kHz; (b) data recorded for directivity experiment at 100 kHz at azimuth 0°, corrected for geometric spreading; (c) data after correction for vertical directivity.

offset ξ_k, the angle of incidence may be computed using $\tan(\varphi_{ik}) = \xi_k/(V_{ijm}.t'_i)$. The traces are corrected for the vertical directivity using

$$s'_{\theta_j z_m}(t'_i, \xi_k) = s_{\theta_j z_m}(t'_i, \xi_k) A^{-1}(t_i | V_{ijm}, \xi_k).$$

2.2 Azimuthal focusing

Despite the narrow window of the receiver module, more than 50% of the maximum amplitude is still recorded at an azimuth of $\pm 50^\circ$ with the source (Fig. 3), and a precise location of the reflectors requires processing the recorded data in order to enhance the resolution. As the arrival times do not depend on the azimuth, the amplitude response measured in the directivity experiment may be used to construct a constant-time azimuthal filter. A smoothed symmetrical curve for $-50^\circ \leq \theta \leq +50^\circ$ is obtained from the directivity diagram at normal incidence, using a moving average and extraction of the even component with respect to azimuth 0°. The curve $A(\theta)$ obtained from the 100 kHz data is shown in Fig. 5(a). Two different processings can be performed using this curve: either an inverse filtering or a non-linear

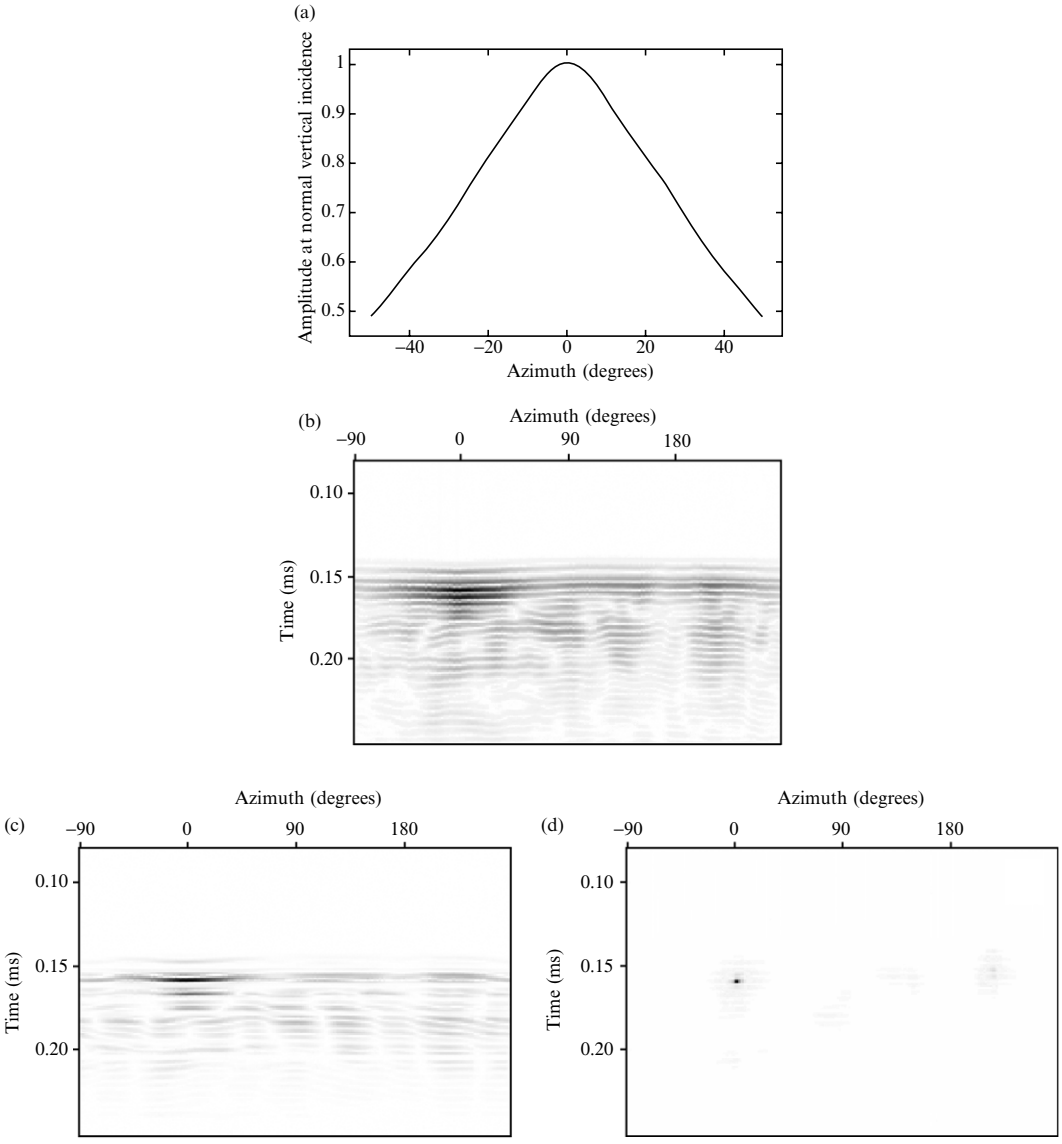

Figure 5 Azimuthal focusing: (a) smoothed directivity curve at 100 kHz; (b) data recorded for directivity experiment at 100 kHz at normal vertical incidence; (c) data filtered by inverse operator; (d) data filtered by non-linear algorithm (in (b), (c) and (d), amplitudes are shown in absolute values with a grey scale).

operation based on a comparison between the observed amplitudes $s_{\xi_k z_m}(t_i, \theta)$ and $A(\theta)$.

The inverse filter is the inverse of the Fourier transform modulus limited to the first spectral zero of $A(\theta)$:

$$s'_{\xi_k z_m}(t_i, \theta) = \mathrm{IFFT}\left(\frac{\mathrm{FFT}\left(\mathrm{s}_{\xi_k \mathrm{z_m}}(\mathrm{t_i}, \theta)\right)}{\|\mathrm{FFT}(\mathrm{A}(\theta))\|_{\text{first lobe}}}\right),$$

where FFT and IFFT represent the fast Fourier transform and the inverse fast Fourier transform, respectively, computed on the variable θ.

The non-linear processing is a time-dependent weight applied at each trace $s_{\xi_k z_m}(t, \theta_j)$. The weight is computed at each time t_i, by comparing the normalized amplitudes of the traces in the range $\theta_j - 50^\circ \le \theta \le \theta + 50^\circ$ with the values of the curve $A(\theta)$:

$$s'_{\xi_k z_m}(t_i, \theta_j) = \frac{s_{\xi_k z_m}(t_i, \theta_j)}{\sum_{\theta=\theta_j-50^\circ}^{\theta_j+50^\circ} \left(\left|\frac{s_{\xi_k z_m}(t_i,\theta)}{s_{\xi_k z_m}(t_i,\theta_j)}\right| - A(\theta - \theta_j)\right)^2}.$$

This formula shows that the weighting factor is the inverse of the mean squared error between observed amplitudes and directivity curve amplitudes. So, if the trace $s_{\xi_k z_m}(t, \theta_j)$ corresponds to an azimuthal receiver location turned towards a reflector, the mean squared error is a minimum at the corresponding reflection time, and the corrected trace $s'_{\xi_k z_m}(t, \theta_j)$ is then amplified relative to other traces and other times for which the mean squared error is greater.

Data recorded at normal vertical incidence during the directivity experiment at 100 kHz are shown in Fig. 5(b). In fact, this experiment was performed over the entire 360° azimuthal range in 2° steps, from − 90° to + 268°. Note that the arrival times are independent of the azimuth: in this example, the standard deviation of the arrival times is lower than 10% of the Ricker wavelet central period. The results of the azimuthal focusing, $s'(t, \theta)$, are shown in Fig. 5(c) for the inverse filtering and in Fig. 5(d) for the non-linear processing. This example demonstrates that the non-linear algorithm is more efficient than the inverse filter, providing an azimuthal directivity of about 25° on processed data.

2.3 Reflected waves enhancement

Strong tube waves propagating along the borehole boundary interfere with the waves reflected from discontinuities in the formation, and in order to get a clear image of the reflectors the tube waves must be filtered out from the data. In practice, this is achieved by both azimuthal focusing and normal moveout correction (NMO) followed by trace stacking. Synthetic data are constructed to illustrate this point, with a source and receiver centred in a borehole, 10 cm in diameter, filled with water having a velocity of 1500 m/s. The offset is varied between 20 and 80 cm, the azimuth covers 360°, and a reflector parallel to the borehole is located in the $\theta = 0^\circ$ direction and 1 m from the borehole boundary in a medium having a velocity of 3000 m/s. A 2D second-order finite-difference modelling for acoustic waves equation is used to simulate the tube waves, generated by a 100 kHz Ricker wavelet. We use the SUFDMOD2 algorithm of the CWP34 library (J.K. Cohen and J.W. Stockwell, CWP Free

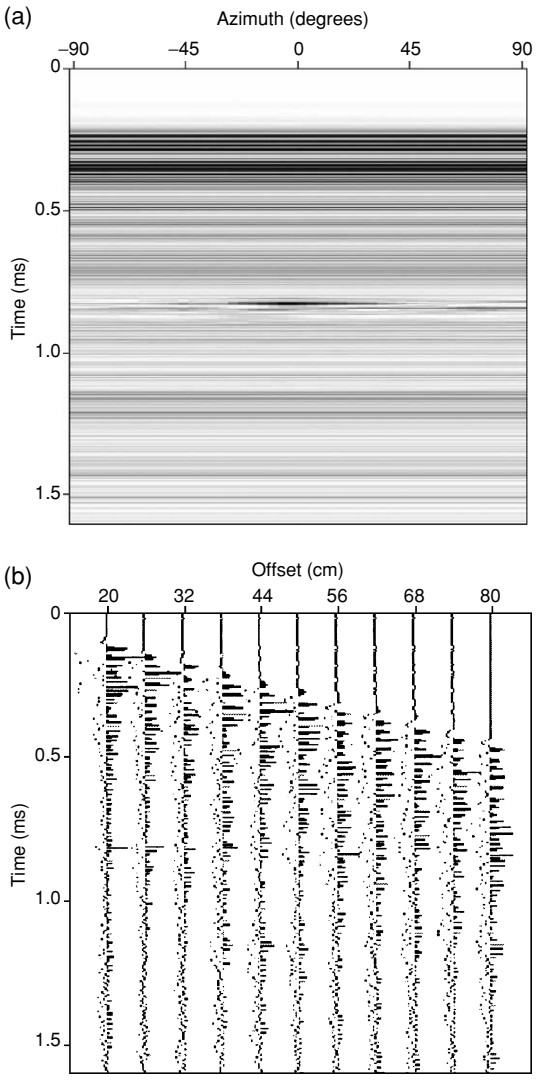

Figure 6 Synthetic data with 'tube waves' and one reflected wave at arrival times of around 0.8 ms from a reflector located towards azimuth 0°: (a) 38 cm common-offset gather (amplitudes drawn in absolute values with a grey scale); (b) 0° common-azimuth gather.

Program, ftp.cwp.mines.edu (138.67.12.4)). Although the acoustic modelling does not account for the shear waves and does not actually simulate borehole waves, the guided waves produced exhibit the main properties relevant to the present study, namely large amplitude and conical geometry of the wavefronts. In this example, we assume that the source and the receiver are precisely centred in a perfectly cylindrical borehole, so that the 'tube waves' do not depend on the

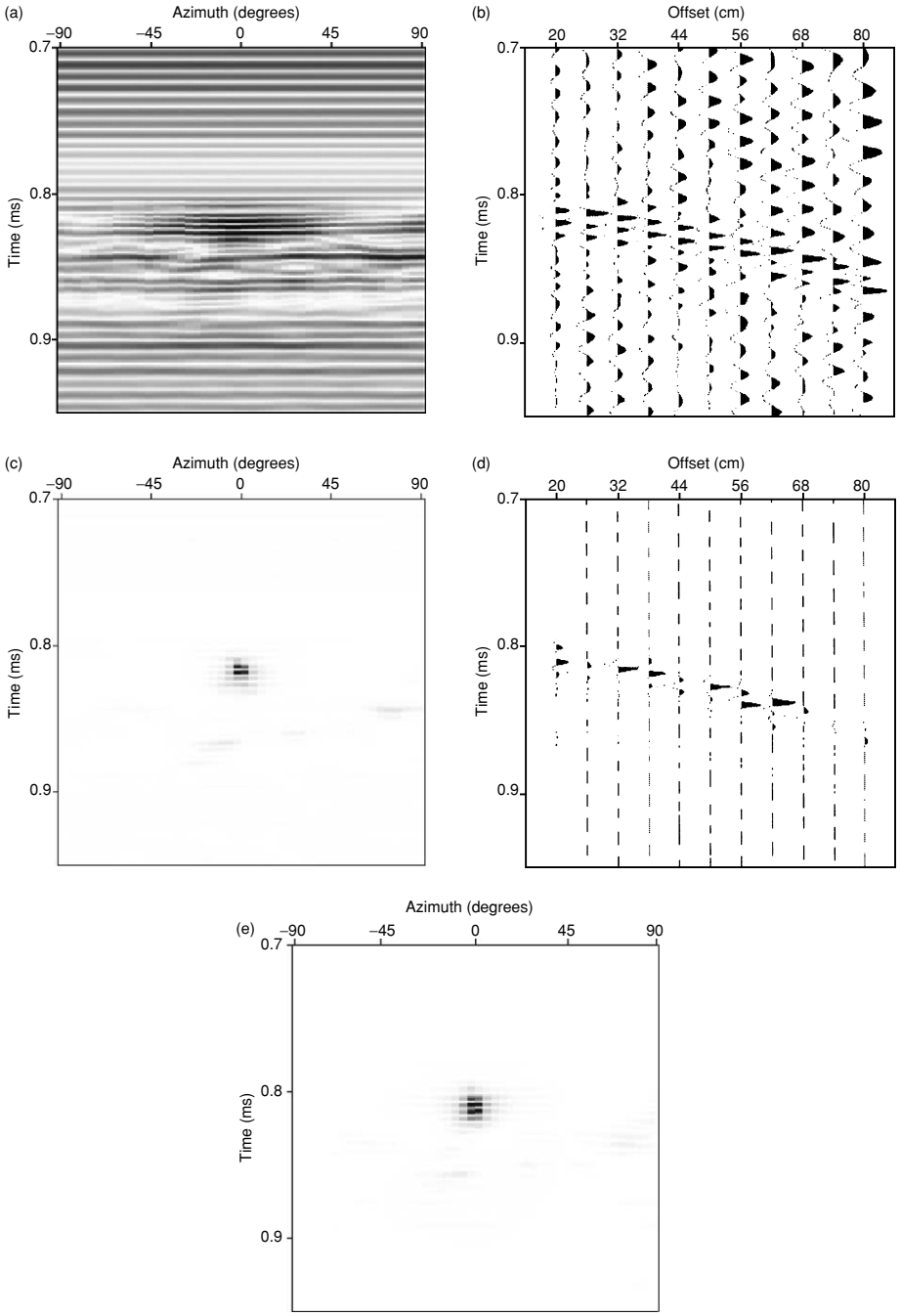

Figure 7 Processing of synthetic data of Fig. 6: (a) initial 38 cm common-offset gather data; (b) initial 0° common-azimuth gather data; (c) and (d) the same data after azimuthal focusing; (e) stack over the 11 offsets after NMO correction (in (a), (c) and (e), amplitudes are shown in absolute values with a grey scale).

azimuth. However, note that the processing results would be the same if the probe were not precisely and/or the borehole were not perfectly cylindrical, which leads to azimuthal variations in the amplitude and the arrival time of the tube waves. The 'reflected' waves are obtained from the data of the directivity experiment carried out at 100 kHz at normal incidence, and they are added to simulated tube waves at the corresponding reflection times. This allows us to assume the amplitude corrections to be made and to take the azimuthal directivity into account. The maximum amplitude of the reflected waves is of the order of the mean amplitude of the tube waves.

Figure 6 shows the synthetic data in a common-offset gather (Fig. 6a, where only the -90° to $+90^\circ$ azimuthal range is drawn), and in a common-azimuth gather (Fig. 6b) corresponding to the azimuth of the reflector. In Fig. 6(b), we see mainly the tube wavetrains arriving along straight lines corresponding to a velocity of 1500 m/s, and we can identify the reflection hyperbola at arrival times around 0.8 ms with a velocity of 3000 m/s. A time zoom of the gathers is shown in Fig. 7(a, b). The azimuthal focusing non-linear algorithm applied to these data (Fig. 7(c, d)) strongly enhances the reflected waves with respect to the tube waves so that, even if they arrive at the same times whatever the azimuth, they do not exhibit amplitude variations similar to the azimuthal directivity curve. Finally, NMO correction applied with a velocity of 3000 m/s to common-azimuth data after azimuthal focusing, and stacking over the whole offset range computed at each azimuth, further enhances the reflection (Fig. 7e).

3 EXPERIMENTAL RESULTS

We now present an experiment performed at a test site in order to illustrate the azimuthal imaging capabilities of the probe and of the associated data processing.

3.1 Test site

A test site was constructed on the Rennes University campus in order to have a controlled medium at typical scales of interest for seismic endoscopy. The test site consists of a well, made of cylindrical tubes of concrete, 8 m in depth and 2.2 m in diameter (Fig. 8). Various objects are placed in

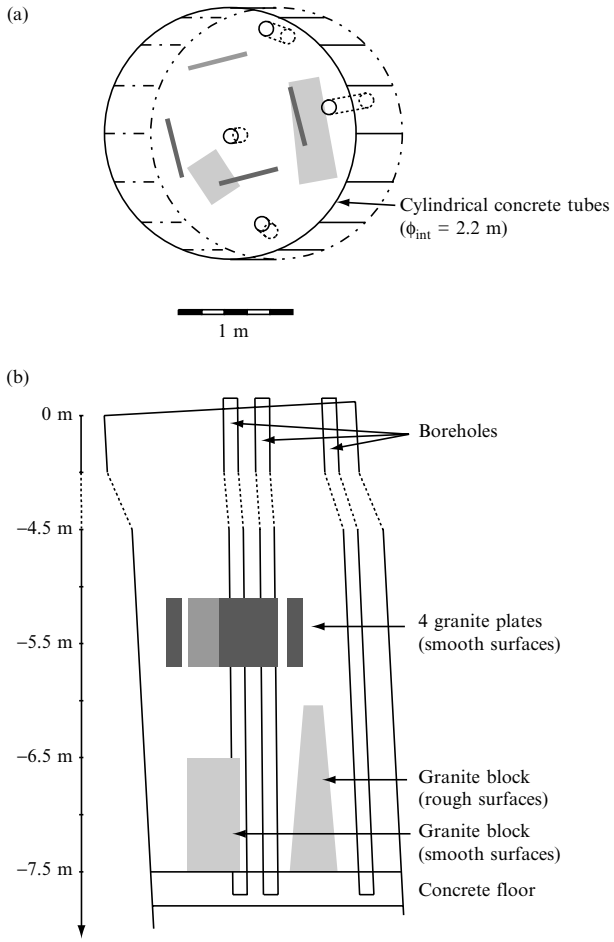

Figure 8 Bottom part of the test site: (a) top view; (b) side view.

Table 1 Parameters used in the experiment at the test site

Granite plates	$z_{min} = -5$ m	$z_{max} = -5.7$ m	
	$\theta = 10^\circ, 100^\circ, 190^\circ, 280^\circ$		
	$d \approx 58$ cm, 66 cm, 56 cm, 38 cm		
Source location	$z_{min} = -4.855$ m	$z_{max} = -6.355$ m	$\delta z = 3$ cm
Receiver location	$\xi_{min} = 29$ cm	$\xi_{max} = 71$ cm	$\delta\xi = 6$ cm
	$\theta_{min} = 0^\circ$	$\theta_{max} = 350^\circ$	$\delta\theta = 10^\circ$
8-fold coverage CMP	$z_{min} = -4.71$ m	$z_{max} = -6$ m	$\delta z = 3$ cm
Source signal	70 kHz Ricker wavelet		
Recorded data	2 ms with 500 kHz sampling frequency		

the well at known locations to provide reflectors (e.g. pieces of rock with smooth or rough surfaces). Four plastic tubes 8 m high and 12 cm in diameter are placed subvertically into the well to act as boreholes.

3.2 Imaging of reflectors

A seismic endoscopy experiment was performed at the test site using the central 'borehole', with water filling the well and the borehole, so that no tube waves were generated. The parameters used in the experiment are summarized in Table 1. Figure 9(a, b) contains the raw data of a CMP corresponding to the depth location of the middle of the plates. Although first arrivals (around 0.35 ms at offset 47 cm) corresponding to direct waves dominate, reflections are visible at times around 0.65, 0.85 (where two reflections are mixed) and 0.95 ms for the offset 47 cm, showing amplitude variations with the azimuth as observed in the directivity diagram. In addition to the processing already discussed (i.e. velocity analysis, amplitude corrections, azimuthal focusing, normal-moveout correction and stack computation), a mute is first applied in order to cancel the first arrivals (above a line from 0.4 ms at offset 29 cm to 0.68 ms at offset 71 cm). Figure 9(c) shows the processed data of the same CMP located at a depth of -5.34 m, obtained with a correction velocity equal to 1470 m/s. Only the reflections corresponding to the four granite plates are clearly visible, well-focused around azimuths 10°, 100°, 190° and 280°. Figure 10 summarizes the results of this experiment, showing the squared amplitudes plotted with the same dynamics in the five pictures, as a function of the reflection distance (traveltime between 0.4 and 1.1 ms converted with a velocity of 1470 m/s) and of the azimuth at the depth -5.34 m (Fig. 10a) or of the depth between -4.89 and -5.82 m at the azimuths 10° (Fig. 10b), 100° (Fig. 10c), 190° (Fig. 10d) and 290° (Fig. 10e). This provides correct 3D imaging of the four granite plates, at known azimuth, depth and radial distance from the probe.

4 CONCLUSIONS

The principle of an acoustic method to perform imaging around boreholes was presented. A probe was designed to acquire seismic data depending on three spatial parameters: the depth, the source–receiver distance and the earring azimuth. This particular acquisition geometry allows us to perform effective data processing, thus enhancing the reflected waves coming from targets located in the vicinity of the borehole. In addition to classical seismic data processing, a

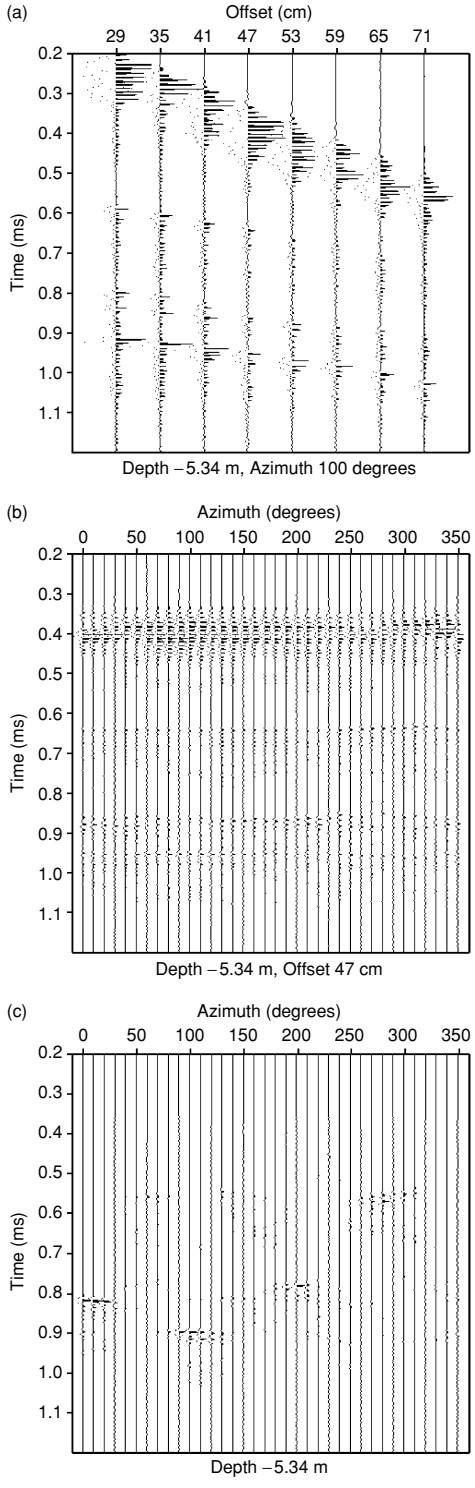

Figure 9 Data from the test site experiment: (a) initial 100° common-azimuth gather data for CMP -5.34 m; (b) initial 47 cm common-offset gather data for CMP -5.34 m; (c) -5.34 m CMP data after processing (mute, amplitude corrections, azimuthal focusing, NMO correction and stack).

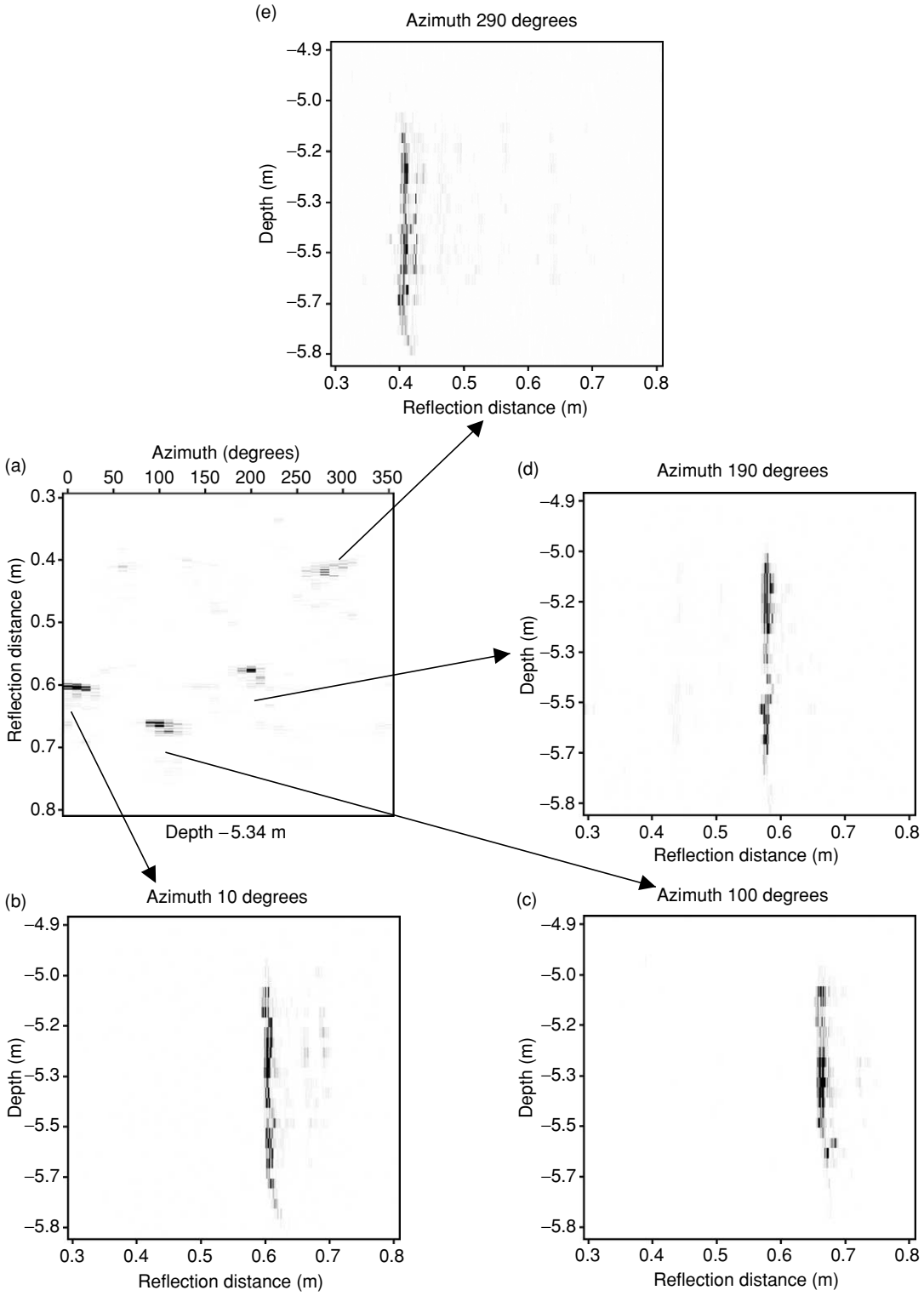

Figure 10 Processed data from the test site experiment, traveltime between 0.4 and 1.1 ms converted into reflection distance with a propagation velocity $V = 1470$ m/s (the squared amplitudes are plotted with the same dynamics): (a) -5.34 m CMP data; (b) 10° common-azimuth gather at depths between -4.89 and -5.82 m; (c) 100° common-azimuth gather at the same depths; (d) 190° common-azimuth gather at the same depths; (e) 290° common-azimuth gather at the same depths.

specific azimuthal focusing algorithm was applied. Clear 3D images of the acoustic discontinuities present in a cylindrical volume surrounding a borehole can be obtained in this way. A test site was constructed in order to perform experiments in a controlled medium, and the first results of seismic endoscopy performed with water as the propagation medium are convincing.

ACKNOWLEDGEMENTS

This work was supported financially by the CNRS and ANDRA through the GdR FORPRO (Research action number 99. II) and corresponds to the GdR FORPRO contribution number 2001/07A. We acknowledge Mr Lemoine of Géosciences Rennes, who helped us in designing equipment for the seismic endoscopy probe. Thanks to Mr Le Merrer of the 'Carrière Clolus' at Lanhélin (Brittany, France), who allowed us to perform preliminary transmission experiments in granite and who gave us the granite samples for our test site.

REFERENCES

Clærbout J.F. 1985. *Imaging the Earth's Interior.* Blackwell Scientific Publications.

Paillet F.L. and Cheng C.H. 1991. *Acoustic Waves in Boreholes*. CRC Press.

Valéro H.P., Sarraco G. and Gibert D. 2001. 3D seismic endoscopy: design of apparatus and basic imaging algorithms. *IEEE Transactions on Geoscience and Remote Sensing* **39**, 2262–2274.